Geol. Mag. **155** (*4*), *2018, pp. 893–906.* © *Cambridge University Press 2016*
doi:10.1017/S0016756816001047

Thermochronology quantifying exhumation history of the Wudang Complex in the South Qinling Orogenic Belt, central China

CHUANBO SHEN*‡†, DI HU*§, CHUN SHAO* & LIANFU MEI*

*Key Laboratory of Tectonics and Petroleum Resources, China University of Geosciences, Ministry of Education, Wuhan 430074, China
‡Faculty of Earth Resources, China University of Geosciences, Wuhan 430074, China
§State Key Laboratory of Lithospheric Evolution, Institute of Geology and Geophysics, Chinese Academy of Sciences, Beijing 100029, China

(*Received* 13 February 2016; *accepted* 13 October 2016; *first published online* 13 December 2016)

Abstract – The Wudang Complex located in the central part of South Qinling, has been inferred to be a segment of the Yangtze Craton involved in the orogen. In this study, the cooling/exhumation history of the Wudang Complex is revealed through combined published geochronology data and new apatite fission-track results. Three rapid exhumation episodes related to relevant geodynamic events have been identified. Previous ^{40}Ar–^{39}Ar and (U–Th)/He data indicate that the most significant exhumation, induced by the collision between the North and South China Blocks, occurred from *c.* 237 to 220 Ma after long-term subsidence and sedimentation of the passive continental margin. The second exhumation event, related to the long-distance effect of the Pacific subduction, occurred during the period from *c.* 126 to 90 Ma. Following the late Cretaceous – Eocene peneplanation stage, the final late Cenozoic exhumation since *c.* 15 Ma may be attributed to the combined effect of the eastward growth of the Tibetan Plateau uplift and the Asian monsoon.

Keywords: thermochronology, fission track, cooling/exhumation, tectonic evolution, Qinling Orogen.

1. Introduction

The Central China Orogenic Belt (CCOB), comprising from west to east the Kunlun, Qilian and Qinling–Dabie Mountains, is a critical zone that separates the northern and southern China continent (Ames, Gaozhi & Baocheng, 1996; Rowley *et al.* 1997; Hacker *et al.* 1998; Xiong *et al.* 2016). As part of the CCOB, the Qinling–Dabie Orogenic Belt (QDOB), which is a collision product of the North China Craton (NCC) and South China Block (SCB), provides important information about the tectonic evolution of the Eastern Asian Continent (Mattauer *et al.* 1985; Şengör, 1985; Ames, Gaozhi & Baocheng, 1996; Rowley *et al.* 1997; Hacker *et al.* 1998; Ratschbacher *et al.* 2000; Hu *et al.* 2006*a*; Dong *et al.* 2011*a*; Zhao *et al.* 2015; Dong & Santosh, 2016; Wu, Xiao & Ma, 2016). Most previous studies focus on two aspects: (1) the continental deep subduction and exhumation process through the ultrahigh-pressure (UHP) metamorphic belt (Ames, Gaozhi & Baocheng, 1996; Hacker *et al.* 2000; Faure *et al.* 2003; Hu *et al.* 2006b; Bader *et al.* 2013*a*, 2013*b*); and (2) the dynamic mechanism of the Triassic collision between the NCC and SCB (Kröner, Zhang & Sun, 1993; Li *et al.* 1993; Okay, Şengör & Satir, 1993; Ratschbacher *et al.* 2006; Dong *et al.* 2012). Earlier studies have generally revealed the geological evolution history of the South Qinling and its affiliation with the break-up of the supercontinent Rodinia (Ling *et al.* 2008, 2010; Bader *et al.* 2013*a*; Yang *et al.* 2013). However, issues including the post-collision evolution process and the timing and amount of exhumation processes are still not clear. Moreover, there is still controversy about the geodynamics of tectonic reactivation and topographic adjustment after the Cretaceous. These scenarios comprise (1) back-arc extension triggered by the subduction of the Pacific plate (Zhou & Li, 2000; Wu *et al.* 2005; Li & Li, 2007; Li *et al.* 2010); (2) a far-field effect of the India–Eurasia collision (Tapponnier *et al.* 2001; Enkelmann *et al.* 2006; Ratschbacher *et al.* 2006; Grave, Buslov & Haute, 2007; Grave *et al.* 2013); and (3) the changing erosion rate, affected by climate since the Miocene (An *et al.* 2001; Guo *et al.* 2002; Clift *et al.* 2008; Allen & Armstrong, 2012).

In this study, we integrate previous geochronology data and our new apatite fission-track (AFT) ages of the Wudang Complex to reconstruct regional thermal history (from break-up, sedimentation, collision, reactivation and cooling to exhumation). These results will help us (1) understand the tectonic–thermal events and related cooling/exhumation processes, and (2) address questions pertinent to the role of Pacific subduction and India–Asia collision in the tectonics of the Yangtze Craton.

2. Geological setting

The Qinling–Dabie Orogenic Belt (QDOB) is a ~2000 km long E–W elongated intra-continental orogeny, connected respectively with Kunlun and

†Author for correspondence: cugshen@126.com

Qilian orogeny to the west and eastern China to the east through the Tanlu fault belt (Fig. 1a). The QDOB developed by the collision between the NCC and SCB in the Triassic. Controlled by the palaeo-Pacific subduction since the Cretaceous and the far-field effects of the India–Asia collision at ~50 Ma (Tapponnier *et al.* 2001; Enkelmann *et al.* 2006; Sharp & Clague, 2006), the QDOB showed intra-continental reactivation throughout the Jurassic to Cenozoic (e.g. Zhang, Vergely & Mercier, 1995; Ratschbacher *et al.* 2003; Dong *et al.* 2011*a*; Dong & Santosh, 2016).

The South Qinling is located between the North Qinling and the northern margin of the SCB (Fig. 1b; Ling *et al.* 2010; Dong & Santosh, 2016). The Wudang terrain is located in the eastern margin of the South Qinling and the western margin of the Nanyang basin that divided the Qinling and Dabie orogenic belt. The Wudang Complex mainly consists of the Neoproterozoic Wudang Group that is unconformity surrounded by the early Neoproterozoic Yaolinghe Group and the Sinian to Phanerozoic sedimentary units (Fig. 2; Ling *et al.* 2008; Yue, Deng & Bagas, 2014).

The Wudang Group is the largest Precambrian suite (~8000 km^2) in the South Qinling and comprises metamorphic volcanic–sedimentary assemblages in greenschist facies, which is subdivided into the Yaoping, Yangping and Shuangtai Formations. This volcanic event may be attributed to the rift-setting according to their bimodal composition (Ling *et al.* 2008, 2010; Xia *et al.* 2008; Li *et al.* 2010). Their geochemical features also suggest this volcanic suite is subduction-related magmatism. Zircon U–Pb dating on the basic volcanic rocks for metarhyolite tuff indicates it formed at ~755 Ma (Table 1; Ling *et al.* 2008), and the laser ablation inductively coupled mass spectrometry (LA-ICP-MS) U–Pb zircon age of meta-acidic volcanic rocks was 668–680 Ma (Y. Zhang *et al.* 2013). The youngest detrital zircon U–Pb age (763 ± 33 Ma) of Shuangtai Formations indicates the timing of the Wudangshan volcanism (Ling *et al.* 2008, 2010). The ^{40}Ar–^{39}Ar ages for hornblende and muscovite are 236.6 ± 0.6 and 231.1 ± 0.9 Ma respectively (Ratschbacher *et al.* 2003), which likely corresponds to the peak metamorphism timing. The Yaolinghe Group contains greenschist facies metamorphosed quartz–keratophyre tuff and pebbly tuff (Zhang *et al.* 2002) and its basaltic volcanisms were dated at *c.* 685 Ma with minor acidic volcanic rocks at *c.* 632 Ma (Cai *et al.* 2007; Ling *et al.* 2008). The widespread doleritic–gabbroic mafic sills emplaced into the Wudang and Yaolinghe Group dated at 679.0 ± 3.1 Ma (Ling *et al.* 2008).

3. Samples and methodology

Seven epimetamorphic sandstone samples were collected from the Wudang Group metamorphic rocks. Sample locations are shown in Figure 1c and elevations are determined by GPS (Table 2). The apatite fractions were separated from the rocks using conventional density and magnetic separation techniques after crushing and sieving. The apatites are divided into two separates, one used for age dating (age group) and the other for confined track-length measurements (length group) (Jonckheere, Ratschbacher & Wagner, 2003; Jonckheere *et al.* 2007). All samples were selected for age dating (age group), and five of them (W1, W3, W5, W6 and WD2A) were used for confined track-length measurements. Apatite grains were mounted in epoxy resin, ground, and polished to expose smooth flat internal surfaces. The fission-track analysis was performed at Bergakademie Freiberg following the methods detailed in Shen *et al.* (2012) and Yang *et al.* (2013).

The age-group apatites were etched in 4.0M HNO_3 for 15 s at 25 °C and the muscovite external detectors in 40 % HF for 30 min at room temperature. We used prismatic sections of Durango standard apatite to ensure that tracks are counted in the same facies in the standards and unknowns (Jonckheere *et al.* 2007). Ages were determined using the ζ-calibration approach (Hurford & Green, 1983; Table 2) from a uranium-glass IRMM540R monitor. The zeta values stem from independent calibrations by counting several Durango and Fish Canyon Tuff apatite age standards (Table 2). Track counting was performed on a prismatic apatite surface with a Zeiss Axioplan microscope at magnification of 625 in transmitted light. The muscovite external detector was repositioned, trackside down, on the apatite mounts in the same position as during irradiation. Fossil tracks were counted by focusing on the underside of the external detector without moving the microscope stage (Jonckheere, Ratschbacher & Wagner, 2003). Where possible, at least 20 crystals of each sample were counted for age determination. The length group apatite was etched for 20 s at 21 °C in 5.5M HNO_3 (Donelick, Ketcham & Carlson, 1999). Track-length measurements were performed at a magnification of 1250 using the Zeiss Axioplan microscope equipped with the Autoscan system; all suitable confined tracks parallel to the prismatic surfaces were measured. Separate mounts for track-length measurements were irradiated with heavy ions at the GSI Helmholtz Centre for Heavy Ion Research, Darmstadt (Germany), to increase the number of etchable confined fission tracks (Jonckheere *et al.* 2007).

4. Results and discussion

4.a. Results and thermal history modelling

The AFT results of seven samples are shown in Table 2; the pooled ages (with 1σ) vary from 76.0 ± 9.0 to 103.7 ± 10.7 Ma with $P(\chi^2) > 0.05$; mean track lengths range from 10.6 ± 0.1 to 11.6 ± 0.1 μm, and mean track length (μm) after c-axis correction spans 12.9 ± 0.1 to 13.6 ± 0.1 μm (Fig. 3). The Dpar (c-axis parallel etch pit diameter) values (Donelick, 1993; Donelick, Ketcham

https://doi.org/10.1017/S0016756816001047 Published online by Cambridge University Press

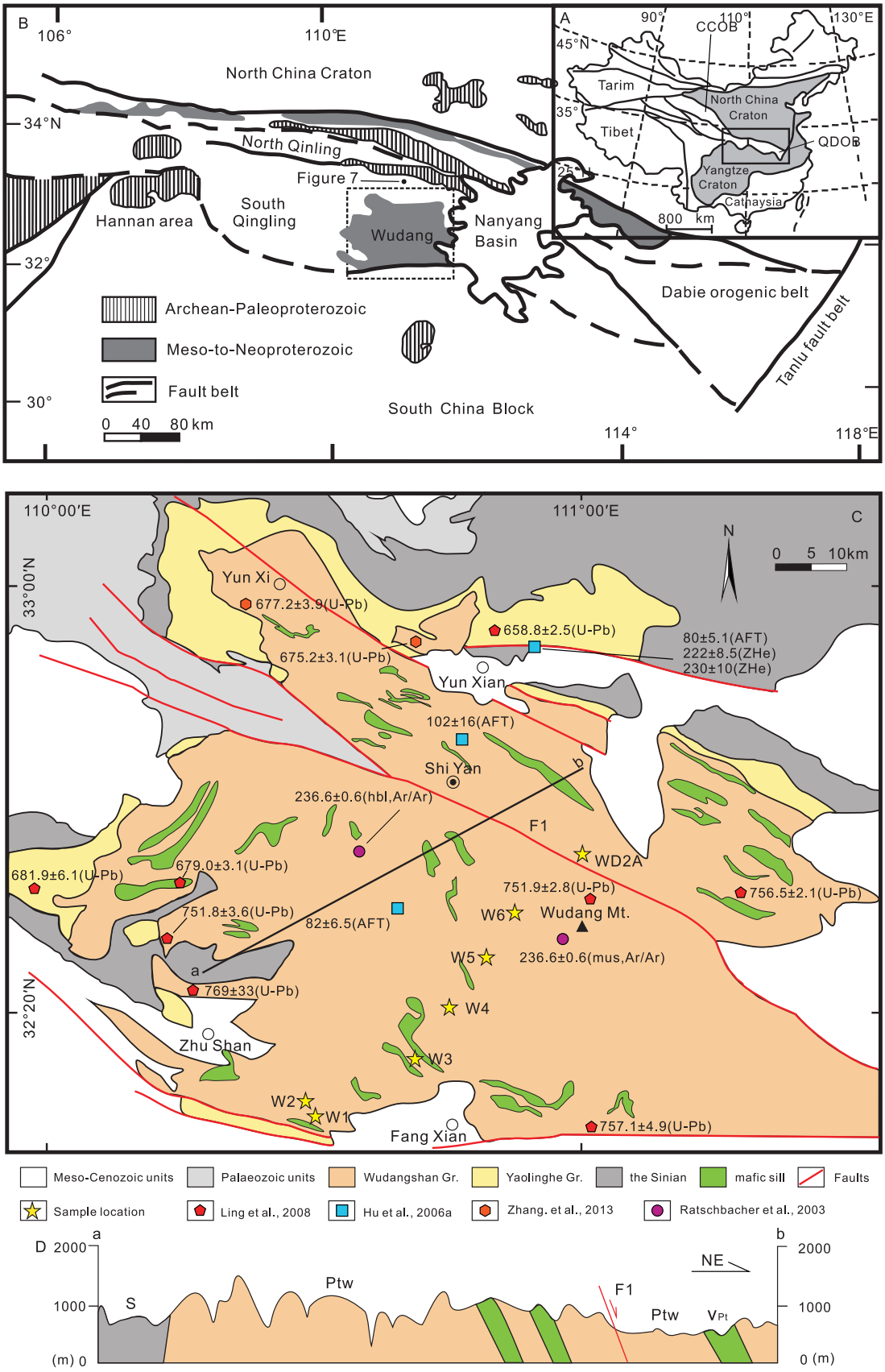

Figure 1. (Colour online) (a) Location of the Qinling–Dabie Orogenic Belt (QDOB), between the North China Craton and Yangtze Craton. (b) Relationships between the Wudang Terrain and adjacent tectonic units (modified from Ling *et al.* 2010). (c) Simplified geological map of the Wudang area modified from Yue, Deng & Bagas (2014) and sample locations. F1: Shiyan fault. (d) Sketch map of tectonic profiles A–B.

https://doi.org/10.1017/S0016756816001047 Published online by Cambridge University Press

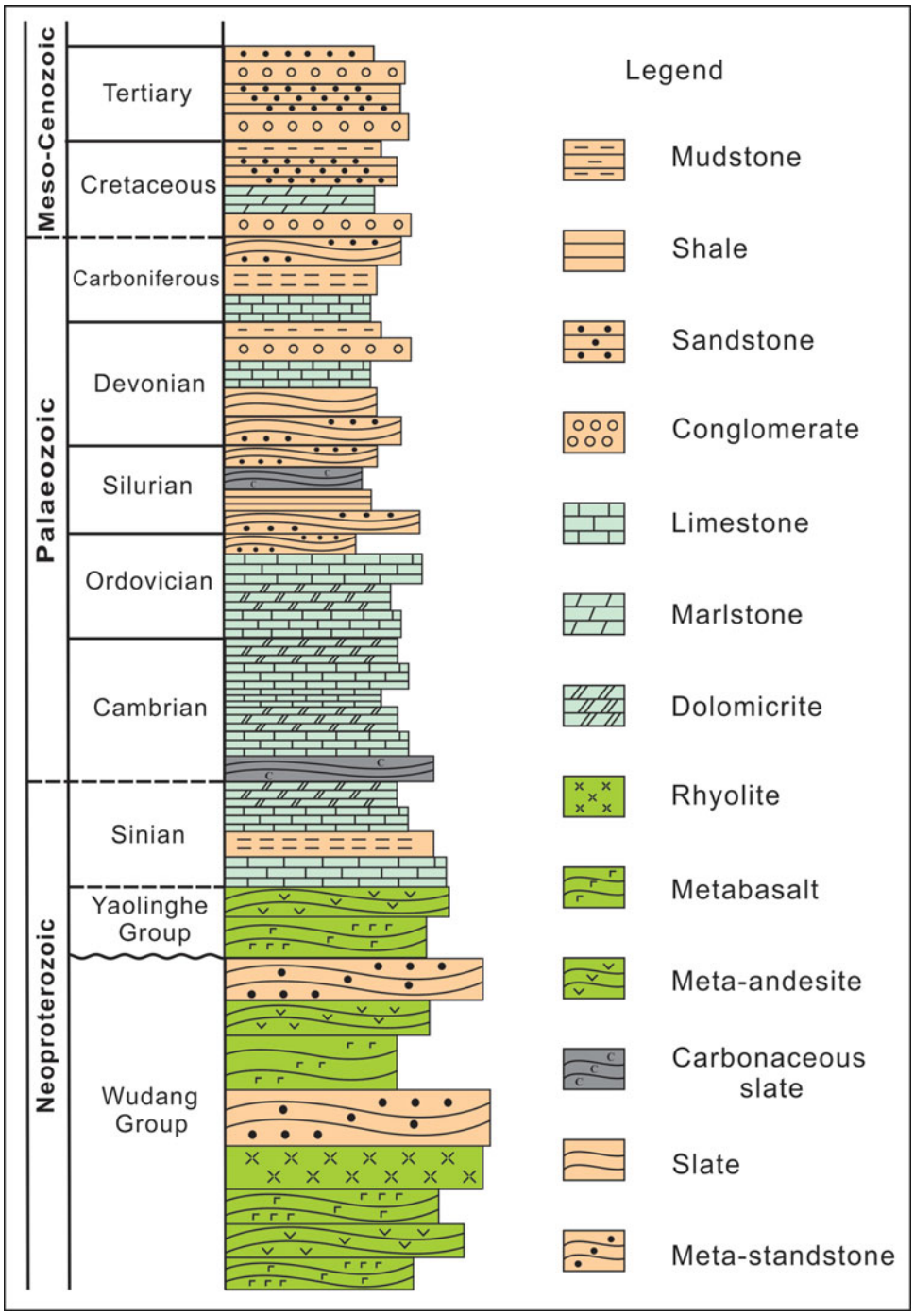

Figure 2. (Colour online) Stratigraphic columns of the Wudang Complex and its adjacent areas (modified from Dong & Santosh, 2016). No vertical scale.

& Carlson, 1999) vary between 2.0 ± 0.3 and 2.5 ± 0.4 μm, which is larger than Durango apatite (1.5–1.9 μm) (McDowell, Mcintosh & Farley, 2005), indicating our samples have higher resistance to thermal annealing (Donelick, O'Sullivan & Ketcham, 2005; Glorie *et al.* 2010).

The AFT age–elevation relationship suggests a relatively slow exhumation rate of *c.* 0.027 mm a^{-1} from *c.* 110 to 80 Ma for elevations below 800 m (Fig. 4). However, sample WD2A which has the youngest ages and the highest elevation, may be affected by the Shiyan fault zone (Fig. 1c). As this fault cut through the Wudang Complex and activated mainly in the Tertiary (Huang, 1993), the apparent age of sample WD2A, located in the hanging wall of the Shiyan fault zone, may be younger. The mean track lengths before c-axis correction decrease from 11.6 to 10.6 μm over a narrow age span (89.0–76.9 Ma), implying that the cooling rate decreased after *c.* 90 Ma (Fig. 3).

The analytic results by Track Age Spectrum Calculation (TASC; Belton & Raab, 2010) could reveal the onset age of cooling. According to annealing characteristics and thermal information recorded on the

https://doi.org/10.1017/S0016756816001047 Published online by Cambridge University Press

Table 1. Compilation of isotopic ages in the Wudang area

Locality	Rock	Mineral for dating	Age (Ma ± 1σ)	Method	Source
Wudangshan	Basic dikes	Zircon	1957 ± 31	TIMS U–Pb	Hu (2004)
Yaolinghe	Volcanic rock	Zircon	632 ± 1	TIMS U–Pb	Cai *et al.* (2007)
Wudangshan	Metarhyolite tuff	Zircon	757.1 ± 4.9	LA–ICP–MS U–Pb	Ling *et al.* (2008)
Wudangshan	Metarhyolite tuff	Zircon	756.5 ± 2.1	LA–ICP–MS U–Pb	Ling *et al.* (2008)
Wudangshan	Metarhyolite tuff	Zircon	751.9 ± 2.8	LA–ICP–MS U–Pb	Ling *et al.* (2008)
Wudangshan	Metarhyolite tuff	Zircon	769.0 ± 3.3	LA–ICP–MS U–Pb	Ling *et al.* (2008)
Wudangshan	Metarhyolite tuff	Zircon	751.8 ± 3.6	LA–ICP–MS U–Pb	Ling *et al.* (2008)
Yaolinghe	Volcanic rock	Zircon	658.8 ± 2.5	LA–ICP–MS U–Pb	Ling *et al.* (2008)
Yaolinghe	Volcanic rock	Zircon	681.9 ± 6.1	LA–ICP–MS U–Pb	Ling *et al.* (2008)
Wudangshan	Mafic sill	Zircon	679.0 ± 3.1	LA–ICP–MS U–Pb	Ling *et al.* (2008)
Wudangshan	Volcanic rock	Zircon	677.2 ± 3.9	LA–ICP–MS U–Pb	Y. Zhang *et al.* (2013)
Wudangshan	Volcanic rock	Zircon	680.4 ± 4.6	LA–ICP–MS U–Pb	Y. Zhang *et al.* (2013)
Wudangshan	Volcanic rock	Zircon	668.4 ± 4.2	LA–ICP–MS U–Pb	Y. Zhang *et al.* (2013)
Wudangshan	Garnet gabbro	Hornblende	236.6 ± 0.6	^{40}Ar—^{39}Ar	Ratschbacher *et al.* (2003)
Wudangshan	Mylonitic granite	Muscovite	231.1 ± 0.9	^{40}Ar—^{39}Ar	Ratschbacher *et al.* (2003)
Wudangshan	Metamorphic rock	Zircon	222.0 ± 8.5	(U–Th–Sm)/He	Hu *et al.* (2006b)
Wudangshan	Metamorphic rock	Zircon	230.0 ± 10	(U–Th–Sm)/He	Hu *et al.* (2006b)
Wudangshan	Metamorphic rock	Apatite	80 ± 5.1	Fission track	Hu *et al.* (2006b)
Wudangshan	Metamorphic rock	Apatite	102 ± 16	Fission track	Hu *et al.* (2006b)
Wudangshan	Metamorphic rock	Apatite	82 ± 11	Fission track	Hu *et al.* (2006b)
Wudangshan	Metamorphic rock	Apatite	89.0 ± 7.1	Fission track	This study
Wudangshan	Metamorphic rock	Apatite	91.6 ± 7.8	Fission track	This study
Wudangshan	Metamorphic rock	Apatite	87.7 ± 5.1	Fission track	This study
Wudangshan	Metamorphic rock	Apatite	103.7 ± 10.7	Fission track	This study
Wudangshan	Metamorphic rock	Apatite	82.0 ± 6.5	Fission track	This study
Wudangshan	Metamorphic rock	Apatite	80.9 ± 5.3	Fission track	This study
Wudangshan	Metamorphic rock	Apatite	76.1 ± 9.0	Fission track	This study

Note: TIMS: thermal ionization mass spectrometry.

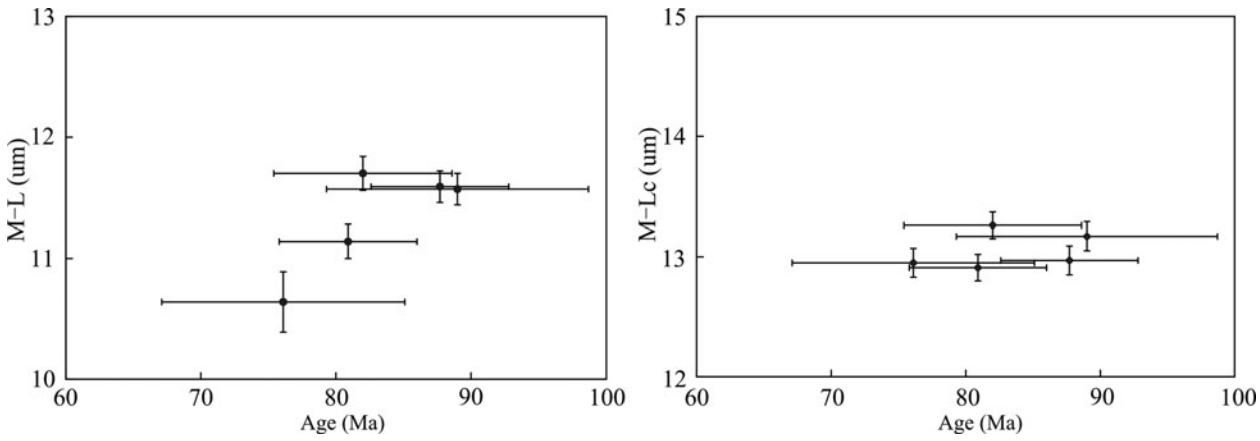

Figure 3. Mean track length (left) and that after c-axis correction (right) (μm) vs apatite fission-track age of the Wudang Complex.

apatite, the track age spectra of samples W1, W3, W5 and W6 (Fig. 5) indicate that the maximum cooling onset ages are 126 ± 10 Ma, 124 ± 7 Ma, 117 ± 9 Ma and 120 ± 8 Ma respectively. These similar ages indicate the initial time when apatite entering the partial annealing zone (PAZ) occurred at ~126 Ma.

The thermal histories (T[t]-paths) of five samples (Fig. 6) were derived through inverse Monte Carlo modelling using the HeFTy software (version 1.8.2; Ketcham, 2005; Ketcham *et al.* 2009) and employing Ketcham, Donelick & Carlson's (1999) annealing model and the c-axis projection of Donelick, Ketcham & Carlson (1999). The initial mean track length of $L_0 = 16.0 \pm 0.8$ μm (Shen *et al.* 2012) was determined from measurements of induced confined tracks in Durango apatite standards. Measured D_{par} values were applied to account for the variation of track length. The Kolmogorov–Smirnov test (GOF) was used to assess the goodness of fit between the modelled and measured results, with thresholds of 0.50 and 0.05 for good and acceptable fits (Ketcham, 2005). In this work, the monotonic path setting was used to allow for both cooling and heating histories. Allowing the samples to cool above the closure temperature of AFT to simulate uncertainty in the initial thermal history, we take 140 °C as the initial constraint. The second constraint is the surface temperature, which we take as 20 °C at 0 Ma. Meantime, at least 500 good paths were modelled for each sample. The inversion modelling results indicate that the samples entered the apatite PAZ rapidly between 126 and 90 Ma, and there then followed a prolonged period with cooling rates <0.5 °C Ma^{-1} residing in the apatite PAZ (Donelick, O'Sullivan & Ketcham, 2005); accelerated cooling has

https://doi.org/10.1017/S0016756816001047 Published online by Cambridge University Press

Table 2. Results of fission-track analysis of apatite from the Wudang Complex

Sample No.	Latitude (N), longitude (E)	Elevation (m)	Lithology	Grains	Ns	Ni	$\zeta \pm 1\sigma$ ($a\,cm^2$)	ρ_d ($10^6\,cm^{-2}$)	P(χ^2) (%)	t-age (Ma $\pm 1\sigma$)	M-L ($\mu m \pm 1\sigma$)	S.D. (M-L)	M-Lc ($\mu m \pm 1\sigma$)	S.D. (M-Lc)	nL	Dpar ($\mu m \pm 1\sigma$)
W1	32° 04.37′ 110° 31.14′	570	Metamorphic rock (Ptw)	20	514	254	278.4 ± 5.1	0.318	100	89.0 ± 7.1	11.57 ± 0.13	1.58	13.17 ± 0.12	1.32	139	2.52 ± 0.03
W2	32° 05.67′ 110° 29.35′	708	Metamorphic rock (Ptw)	47	1761	850	278.4 ± 5.1	0.320	68.8	91.6 ± 7.8	–	–	–	–	–	–
W3	32° 08.43′ 110° 42.55′	471	Metamorphic rock (Ptw)	34	844	550	285.6 ± 4.2	0.403	100	87.7 ± 5.1	11.59 ± 0.13	1.28	12.97 ± 0.12	1.21	104	2.05 ± 0.02
W4	32° 17.65′ 110° 45.11′	757	Metamorphic rock (Ptw)	16	421	162	278.4 ± 5.1	0.289	97.6	103.7 ± 10.7	–	–	–	–	–	–
W5	32° 20.94′ 110° 49.53′	391	Metamorphic rock (Ptw)	18	528	260	278.4 ± 5.1	0.292	96.5	82.0 ± 6.5	11.70 ± 0.14	1.44	13.26 ± 0.11	1.12	101	2.01 ± 0.03
W6	32° 22.62′ 110° 51.96′	309	Metamorphic rock (Ptw)	24	631	447	285.6 ± 4.2	0.404	86.9	80.9 ± 5.3	11.14 ± 0.14	1.30	12.91 ± 0.11	1.14	82	1.98 ± 0.03
WD2A	32° 24.99′ 111° 01.09′	936	Metamorphic rock (Ptw)	31	206	119	261.8 ± 6.2	0.338	99.9	76.1 ± 9.0	10.64 ± 0.25	2.51	12.95 ± 0.12	1.25	63	2.52 ± 0.03

Note: Grains: number of measured grains; Ns: number of spontaneous tracks; Ni: number of induced tracks; ζ: ζ calibration factor; ρ_d: track density in standard uranium glass; P(χ^2): chi-square probability; t-age: fission track age, using pooled ages; 1σ: standard error; M-L: mean track length; S.D.: standard deviation; M-Lc: mean track length after c-axis correction; nL: number of measured confined tracks; Dpar: mean etch pit diameter; Ptw: Proterozoic Wudang Group; –: no data

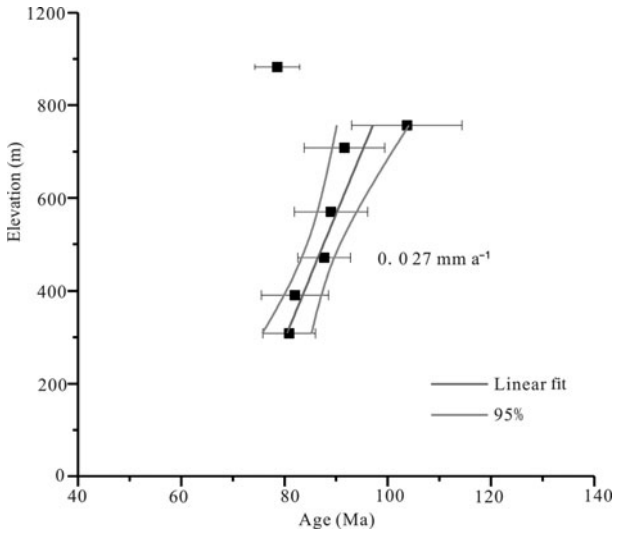

Figure 4. AFT age–elevation relationship in the Wudang area.

occurred at an average cooling rate of ~3 °C Ma^{-1} since *c.* 15 Ma.

4.b. The cooling/exhumation history reconstruction

According to distinct closure temperatures of different minerals, the multiple geochronometers allow us to reconstruct the thermal history of a rock unit (e.g. Glorie *et al.* 2010; Dong *et al.* 2011*b*; Shen *et al.* 2012). Figure 7 shows age vs closure temperature plots, illustrating the multi-stage cooling/exhumation process of the Wudangshan Complex. The zircon U–Pb, hornblende ^{40}Ar–^{39}Ar, muscovite ^{40}Ar–^{39}Ar and ZHe (zircon (U–Th/He) data were used to constrain the cooling process under medium-high temperature (>200 °C). The T[t]-paths based on the AFT data (Fig. 6) were used to reveal the cooling procedure at low temperature (<120 °C). Integrating all these data (Table 1), the thermal history of the Wudangshan Complex can be divided into seven stages: (1) Stage I – the temperature decreased from the closure temperature (700–800 °C; Cherniak & Watson, 2003) of the U–Pb zircon system to the surface condition (~20 °C) from *c.* 755 to *c.* 632 Ma at a fast cooling rate of *c.* 5.7 °C Ma^{-1}. (2) Stage II – the temperature rose rapidly to the hornblende ^{40}Ar–^{39}Ar system (450–550 °C; McDougall & Harrison 1999) from *c.* 632 Ma to *c.* 237 Ma. (3) Stage III – the volcanic rocks are recorded as cooling through temperatures of the ZHe system (180–220 °C; Reiners *et al.* 2004) between *c.* 237 and *c.* 220 Ma at a rate of *c.* 17.6 °C Ma^{-1} which means that exhumation rate may reach 0.4 km Ma^{-1}. (4) Stage IV – from the ZHe system (180–220 °C) to the closure temperature (~120 °C) of AFT (Ketcham, Donelick & Carlson, 1999) between *c.* 220 and *c.* 126 Ma at a decreasing cooling rate of *c.* 0.8 °C Ma^{-1}. (5) Stage V – the sample cooled through the apatite PAZ from 126 to 90 Ma at a rate of *c.* 1.5 °C Ma^{-1}. (6) Stage VI – the slowest cooling stage according to the thermal modelling results (Fig. 6) occurred from *c.* 90 to *c.* 15 Ma at an insignificant speed. (7) Stage VII – a final accelerated cooling to the surface temperature (20 °C) occurred from *c.* 15 Ma to the present at a rate of *c.* 3 °C Ma^{-1}, corresponding to an exhumation rate of *c.* 0.1–0.15 km Ma^{-1}.

4.c. Geodynamic interpretations

The thermal history of the Wudang Complex recorded by the thermochronological data is related to the geodynamic setting and tectonic evolution of the South Qinling orogenic belt. The volcanic suite of the Wudang Group was formed at *c.* 755 Ma dating by the zircon U–Pb method (Ling *et al.* 2008, 2010), and this rift-related igneous event indicated a complete separation of the South China Block and a break-up of the supercontinent Rodinia (Ling *et al.* 2008, 2010; Xia *et al.* 2008; Bader *et al.* 2013*a*). The weathered unconformity between the Wudang Group and the Yaolinghe Group indicates that the Wudang rocks were exposed at the surface in Neoproterozoic times (Huang, 1993). Similarly, the disconformities contact between the Yaolinghe Group and the Sinian carbonate formation indicates that the Yaolinghe volcanic suite had experienced the same cooling event. Therefore, a rapid cooling process (stage I) through heat exchange with the surrounding rock can be assumed from *c.* 755 Ma to *c.* 632 Ma. This event was followed by a long-term extension and subsidence process under the passive continental margin setting (stage II), which resulted in >10 km sediments from the end of the Neoproterozoic to the mid-Triassic (Fig. 2; Hu, 2004). The rocks of the Wudang Group located at the bottom may experience regional metamorphism due to the deep burial depth.

A rapid decrease occurred in the thermal history (stage III) after a long-time sedimentation (Fig. 7), indicating the collision event between the NCC and SCB with intensive deformation and rapid exhumation. The Triassic orogenic event induced by the subduction of the Yangtze plate under the NCC has significant impacts on the entire Qinling–Dabie Belt, North China Craton and South China Block (Ratschbacher *et al.* 2003, 2006; Hu *et al.* 2006*a*, 2006*b*). Many pre-existing shear/fault zones (Lonan, Shangxiang, Shangdan) have been reactivated in the North Qinling between 200 and 240 Ma (Ratschbacher *et al.* 2003). The UHP rocks were formed at ~240 Ma and quickly returned in the Tongbai–Dabie area due to the delamination of the lithospheric mantle (Hu *et al.* 2006b; Zhang, Ma & Holtz, 2010). The Wudang Complex was part of the Yangtze Craton, and the rapid extensional exhumation allowed these greenschist rocks to be exposed on the surface.

The decreasing cooling, at *c.* 0.8 °C Ma^{-1}, from *c.* 220 to 126 Ma (stage IV; Fig. 7) clearly reflects a gravitational adjustment after the rapid exhumation during orogeny, which is also in accordance with the slight deformation and sedimentation investigated in the Qinling area from the Jurassic to the Early Cretaceous (Ratschbacher *et al.* 2006). After that, the inversion

https://doi.org/10.1017/S0016756816001047 Published online by Cambridge University Press

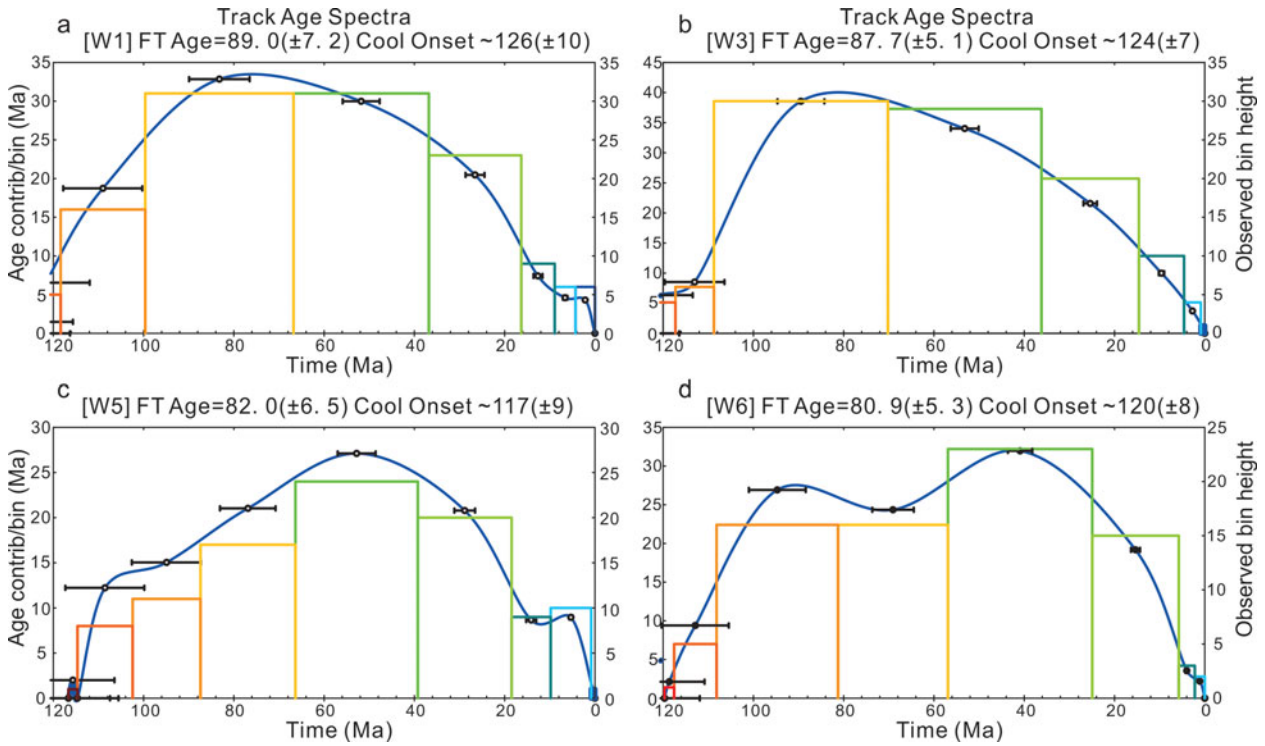

Figure 5. (Colour online) Onset ages of apatite cooling analysed by Track Age Spectrum Calculation (TASC; Belton & Raab, 2010).

modelling results according to the AFT data indicate that the samples passed rapidly through the apatite PAZ between 126 Ma and 90 Ma (stage V). Previous studies have already indicated that the late Jurassic – early Cretaceous tectonic-reactivated and magmatism throughout eastern China (e.g. Tongbai–Dabie, Yangtze craton and eastern NCC (Hacker *et al.* 1998; Wu *et al.* 2005; Li & Li, 2007; Chen *et al.* 2009; Li *et al.* 2010; Zhang, Ma & Holtz, 2010; Xie, Mao & Zhao, 2011)) were induced by the subduction of the palaeo-Pacific plate (Wu *et al.* 2005; Zhou *et al.* 2006; Huang *et al.* 2007; Chen *et al.* 2009; Zhang *et al.* 2011). Hu *et al.* (2006b) also related the large-scale transtensional deformation between ~140 and 110 Ma observed in the Tongbai–Dabie region to the subduction of the Pacific Plate. Hence, the Pacific back-arc extension could contribute to entering the apatite PAZ from *c.* 126 to 90 Ma despite the large distance to the coast.

Stage VI is characterized by very slow cooling or even reheating during the late Cretaceous – Eocene, but local burial in the sedimentary basin and rapid erosion in the edge shoulder occurred (Shen *et al.* 2012). For example, the Late Cretaceous – Eocene red bed deposition in pull-apart basins occurred in eastern China (e.g. Arne *et al.* 1997; Ratschbacher *et al.* 2006) coeval with widespread Cretaceous strike-slip and extensional deformation in eastern Asia (Hacker *et al.* 2000; Ratschbacher *et al.* 2000, 2003; Enkelmann *et al.* 2006). This peneplanation stage is widespread from the eastern Tibetan Plateau to eastern China including the Sichuan basin (Richardson *et al.* 2008; Deng *et al.* 2013; Tian *et al.* 2013, 2015), the Yangtze Craton (Hu *et al.* 2006*a*; Shen *et al.* 2012) and the Qinling–Dabie orogen (Enkelmann *et al.* 2006; Hu *et al.* 2006b; Ratschbacher *et al.* 2006; Heberer *et al.* 2014). The peneplanation period in the South Qinling region initiated at *c.* 90 Ma, which is similar to the Hannan–Micang massif (Tian *et al.* 2012; Yang *et al.* 2013) but different from the Sichuan basin (Shen, Mei & Xu, 2009; Deng *et al.* 2013), the middle-Yangtze craton (Shen *et al.* 2011, 2012) and the Dabie orogenic belt (Hu *et al.* 2006b). A regional low-relief landscape across the eastern Tibetan Plateau and much of central China may also have resulted in this thermal stagnation period (Arne *et al.* 1997; Kirby *et al.* 2002; Ratschbacher *et al.* 2003, 2006; Enkelmann *et al.* 2006; Deng *et al.* 2013).

The final accelerated cooling since *c.* 15 Ma (stage VII; Fig. 7) has also been documented (Fig. 8a), in the eastern Tibetan Plateau (Clark *et al.* 2005; Ouimet *et al.* 2010), the Longmen Shan (Arne *et al.* 1997; Tian *et al.* 2013), the Sichuan Basin (Shen, Mei & Xu, 2009; Deng *et al.* 2013), the Hannan–Micang massif (Tian *et al.* 2012; Yang *et al.* 2013), the Daba Shan (Z. Zhang *et al.* 2013; Yang, 2014), the Qinling (Enkelmann *et al.* 2006; Hu *et al.* 2006b) and even northern Kyrgyz Tien Shan (Glorie *et al.* 2010; Macaulay *et al.* 2014). Most previous studies suggest that this rapid cooling since *c.* 15 Ma is due to the eastward growth of the Tibetan Plateau after the collision of India and Asia (Tapponnier *et al.* 2001; Liu, Cui & Liu, 2004; Clark *et al.* 2005; Enkelmann *et al.* 2006; Tian *et al.* 2012; Macaulay *et al.* 2014). The unconformity between Eocene and Neogene in the adjacent basin (Fig. 8c) supports this event. Tada, Zheng &

https://doi.org/10.1017/S0016756816001047 Published online by Cambridge University Press

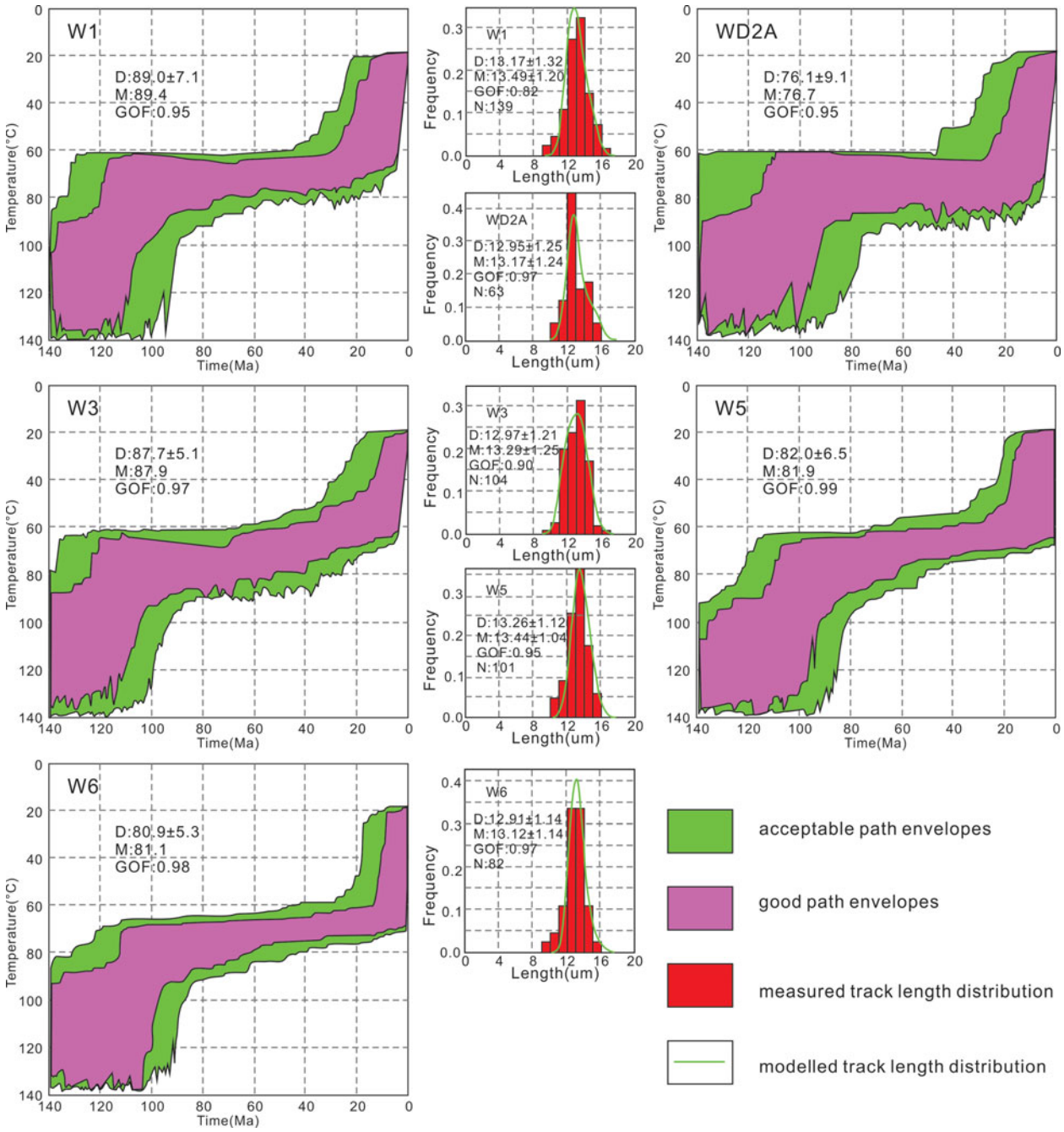

Figure 6. (Colour online) Low-temperature thermal history and confined track-length distribution modelling by the HeFTy 1.8.2 software (Ketcham, 2005; Ketcham *et al.* 2009) based on AFT data. D, determined apatite fission-track age (in Ma with 1σ error) and mean confined track length (in μm with standard deviation). M, modeled apatite fission-track age and mean confined track length. N, number of measured confined track lengths. GOF is the Kolmogorov–Smirnov test, assessing the fit between the modelled and measured results, with thresholds of 0.05 and 0.50 for good and acceptable fits (Ketcham, 2005).

Clift (2016) attributed the uplift of the northern and eastern Tibetan Plateau at *c.* 15–10 Ma to lower crustal flow, which is due to crustal thickening and northeastward expansion of the partial melting materials (Clark & Royden 2000; Yuan *et al.* 2013). However, we also cannot ignore the influence of climate change on the rapid exhumation and landscape adjustment because this exhumation process coincides with the regional climate change in East Asia (Fig. 8b; Allen & Armstrong, 2012). Late Cenozoic global cooling and the onset of the Asian monsoon in the early Miocene have been widely cited for Himalayan–Tibet uplift (Guo *et al.* 2002; Clift *et al.* 2008; Armstrong & Allen, 2011; Allen & Armstrong, 2012). The East Asian monsoon climate has been mainly dominated by the widespread East Asian summer monsoon (EASM) since the Miocene, characterized by high moisture levels and heavy summer rainfall (Guo *et al.* 2008; Molnar, Boos & Battisti, 2010). The South Qinling area located in the south of the Chinese loess plateau developed rich river and rainfall that induced rapid erosion. The famous Three Gorges is the consequence of incision by the Yangtze

https://doi.org/10.1017/S0016756816001047 Published online by Cambridge University Press

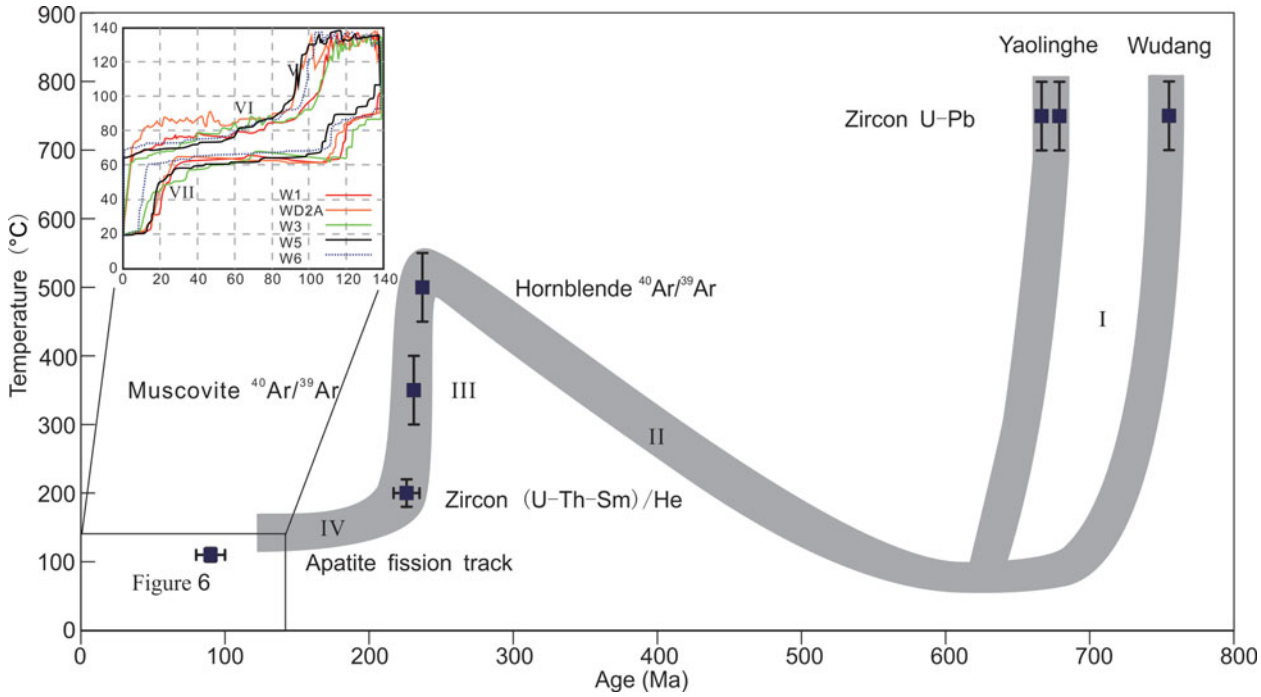

Figure 7. (Colour online) Cooling paths for the Wudangshan Complex using multiple thermochronological methods including zircon U–Pb, ^{40}Ar–^{39}Ar, ZHe and AFT. The data are shown in Table 1 and Figure 1c.

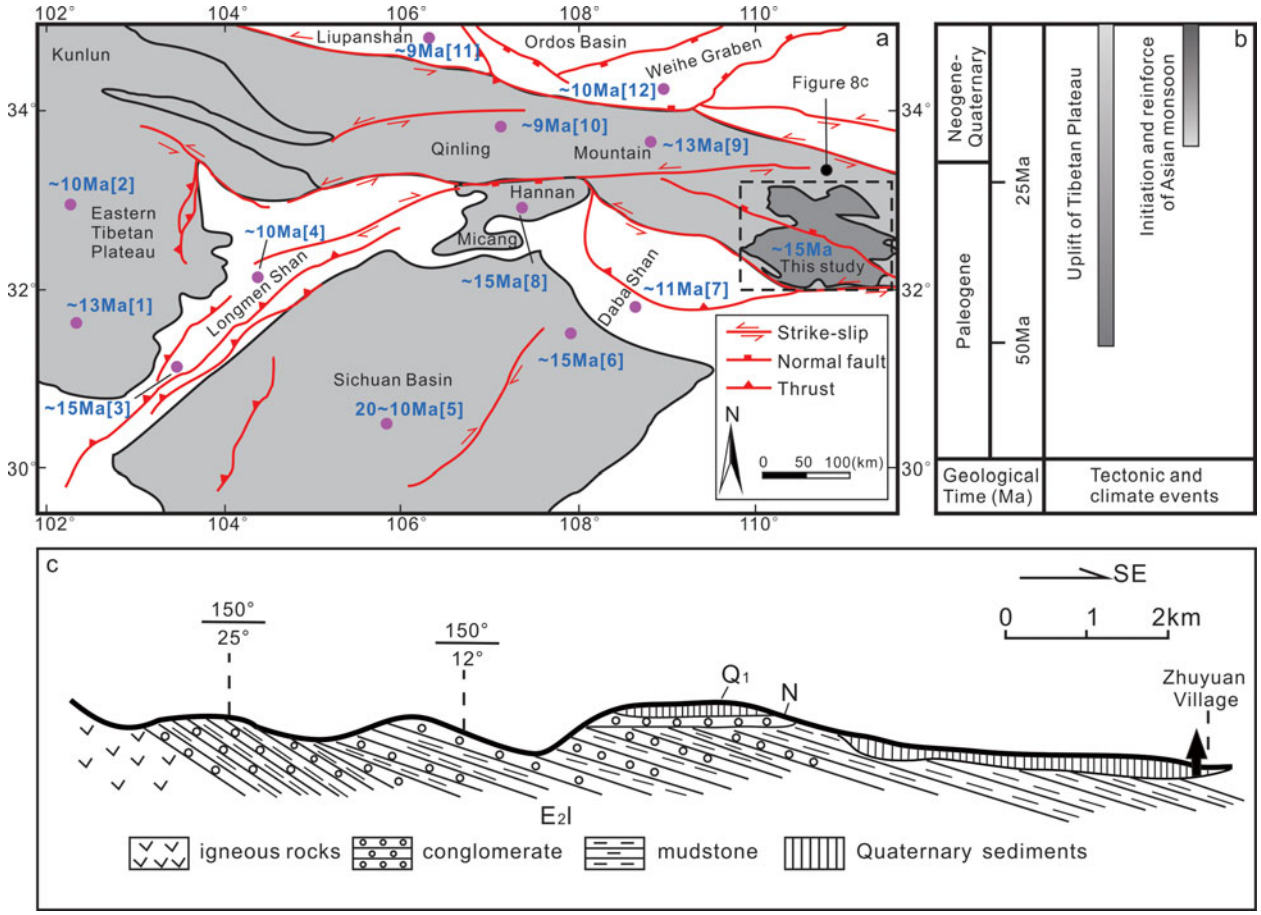

Figure 8. (Colour online) (a) Simplified geological map showing the regional denudation event after *c.* ~15 Ma. Reference codes are [1] = Clark *et al.* (2005); [2] = Ouimet *et al.* (2010); [3] = Tian *et al.* (2013); [4] = Arne *et al.* (1997); [5] = Deng *et al.* (2013); [6] = Shen, Mei & Xu (2009); [7] = Zhang *et al.* (2006); [8] = Tian *et al.* (2012); and Yang *et al.* (2013); [9] =Wang *et al.* (2011); [10] = Enkelmann *et al.* (2006); [11] = Lin *et al.* (2010); and [12] = Liu *et al.* (2013). (b) Possible geodynamic mechanism of the late-Cenozoic tectonic and climate events. (c) Discontinuity of Lushi basin located in the northeast of the Wudang Terrain between Eocene and Neogene. Location of Lushi basin is shown in Figure 1b.

https://doi.org/10.1017/S0016756816001047 Published online by Cambridge University Press

River, and similar river incision also occurred in the central Sichuan Basin and Yangtze River Delta (Kirby *et al.* 2002; Richardson *et al.* 2008; P. Zhang *et al.* 2013). Hence, we may not exclude the effect of the Asian monsoon from the Late Miocene to the present on enhanced exhumation/cooling, although as a secondary cause with respect to tectonic activity.

5. Conclusions

Tectonic evolution of the South Qinling orogenic belt was clarified through joint analysis of previous multiple geochronologic data and our new AFT data from the Wudang Complex. A gravitational adjustment period from *c.* 220 to 126 Ma occurred after the fierce exhumation in the Triassic due to collision between the NCC and SCB, which was a response to minor tectonism and sedimentation in the Qinling area during Jurassic to Early Cretaceous time. Meantime, the South Qinling area could also be affected by Pacific subduction to induce the apatite cooling through the PAZ from *c.* 126 to *c*. 90 Ma. The AFT thermal history modelling indicates the late Cretaceous – Eocene peneplanation stage is characterized by insignificant exhumation, coinciding with the formation of regional low-relief landscape. The widespread late Cenozoic accelerated cooling has taken place since 15 Ma in the South Qinling area. It could be influenced by the eastward growth of the Tibetan Plateau uplift and the Asian monsoon as a combined effect of endogenic and exogenic geological process.

Acknowledgements. This work was supported by the National Natural Science Foundation of China (No. 41372140, 40902038), the Fundamental Research Fund for the Central Universities, China University of Geosciences (Wuhan, No. 201536), the Outstanding Youth Funding of Natural Science Foundation of Hubei Province (No. 2016CFA055) and the Wuhan Science and Technology Project (No. 2016070204010145). We are very grateful to Professor Lothar Ratschbacher, Dr Raymond Jonckheere, Dr Zhao Yang and Dr Bastian Wauschkuhn for their kind help with and discussion of fission-track analysis; Professor Richard Ketcham for providing the HeFTy software; Dr Adam Szulc, Dr Tom Wittenschlaeger and Dr Xiang Ge for polishing the English; and Editor-in-Chief, Professor Allen Mark and three anonymous reviewers for their comments and suggestions. Shen's stay at Freiberg was funded by the China Scholarship Council.

References

Allen, M. B. & Armstrong, H. A. 2012. Reconciling the intertropical convergence zone, Himalayan/Tibetan tectonics, and the onset of the Asian monsoon system. *Journal of Asian Earth Sciences* **44**(1), 36–47.

Ames, L., Gaozhi, Z. & Baocheng, X. 1996. Geochronology and isotopic character of ultrahigh-pressure metamorphism with implications for collision of the Sino-Korean and Yangtze cratons, central China. *Tectonics* **15**(2), 472–89.

An, Z., Kutzbach, J. E., Prell, W. L. & Porter, S. C. 2001. Evolution of Asian monsoons and phased uplift of the Himalaya-Tibetan plateau since Late Miocene times. *Nature* **411**(6833), 62–6.

Armstrong, H. A. & Allen, M. B. 2011. Shifts in the intertropical convergence zone, Himalayan exhumation, and late Cenozoic climate. *Geology* **39**(1), 11–14.

Arne, D., Worley, B., Wilson, C., She, F. C., Foster, D., Zhi, L. L., Shu, G. L. & Dirks, P. 1997. Differential exhumation in response to episodic thrusting along the eastern margin of the Tibetan Plateau. *Tectonophysics* **280**(3–4), 239–56.

Bader, T., Franz, L., Ratschbacher, L., Capitani, C. D., Webb, A. A. G., Yang, Z., Pfänder, J. A., Hofmann, M. & Linnemann, U. 2013a. The Heart of China revisited: II Early Paleozoic (ultra)high-pressure and (ultra)high-temperature metamorphic Qinling orogenic collage. *Tectonics* **32**(4), 922–47.

Bader, T., Ratschbacher, L., Franz, L., Yang, Z., Hofmann, M., Linnemann, U. & Yuan, H. 2013b. The Heart of China revisited, I. Proterozoic tectonics of the Qin Mountains in the core of supercontinent Rodinia. *Tectonics* **32**(3), 1497–505.

Belton, D. X. & Raab, M. J. 2010. Cretaceous reactivation and intensified erosion in the Archean–Proterozoic Limpopo Belt, demonstrated by apatite fission track thermochronology. *Tectonophysics* **480**(s 1–4), 99–108.

Cai, Z., Xiong, X., Hong, L., Dekuang, W. U., Sun, S. & Rao, B. 2007. Forming age of the volcanic rocks of the Yaolinghe Group from Wudang Block,Southern Qinling Mountain: constraint from grain-zircon U-Pb dating. *Acta Geologica Sinica* **81**(5), 620–5.

Chen, L., Ma, C. Q., She, Z. B., Mason, R., Zhang, J. Y. & Zhang, C. 2009. Petrogenesis and tectonic implications of A-type granites in the Dabie orogenic belt, China: geochronological and geochemical constraints. *Geological Magazine* **146**(5), 638–51.

Cherniak, D. J. & Watson, E. B. 2003. Diffusion in zircon. *Physics & Chemistry of Minerals* **53**, 113–39.

Clark, M. K., House, M. A., Royden, L. H., Whipple, K. X., Burchfiel, B. C., Zhang, X. & Tang, W. 2005. Late Cenozoic uplift of southeastern Tibet. *Geology* **33**(6), 525–38.

Clark, M. K. & Royden, L. H. 2000. Topographic ooze: building the eastern margin of Tibet by lower crustal flow. *Geology* **28**(8), 703–6.

Clift, P. D., Hodges, K. V., Heslop, D., Hannigan, R., Long, H. V. & Calves, G. 2008. Correlation of Himalayan exhumation rates and Asian monsoon intensity. *Nature Geoscience* **1**(12), 875–80.

Deng, B., Liu, S. G., Li, Z. W., Jansa, L. F., Liu, S., Wang, G. Z. & Sun, W. 2013. Differential exhumation at eastern margin of the Tibetan Plateau, from apatite fission-track thermochronology. *Tectonophysics* **591**, 98–115.

Donelick, R. A. 1993. Method of fission track analysis utilizing bulk chemical etching of apatite. US Patent No. 5267274.

Donelick, R. A., Ketcham, R. A. & Carlson, W. D. 1999. Variability of apatite fission-track annealing kinetics: II. Crystallographic orientation effects. *American Mineralogist* **84**, 1224–34.

Donelick, R. A., O'Sullivan, P. B. & Ketcham, R. A. 2005. Apatite fission-track analysis. *Reviews in Mineralogy & Geochemistry* **58**, 49–94.

Dong, Y., Genser, J., Neubauer, F., Zhang, G., Liu, X., Yang, Z. & Heberer, B. 2011a. U-Pb and $^{40}Ar/^{39}Ar$ geochronological constraints on the exhumation history

https://doi.org/10.1017/S0016756816001047 Published online by Cambridge University Press

of the North Qinling terrane, China. *Gondwana Research* **19**(4), 881–93.

Dong, Y., Liu, X., Zhang, G., Chen, Q., Zhang, X., Li, W. & Yang, C. 2012. Triassic diorites and granitoids in the Foping area: constraints on the conversion from subduction to collision in the Qinling orogen, China. *Journal of Asian Earth Sciences* **47**(1), 123–42.

Dong, Y. P. & Santosh, M. 2016. Tectonic architecture and multiple orogeny of the Qinling Orogenic Belt, Central China. *Gondwana Research* **29**(1), 1–40.

Dong, Y., Zhang, G., Neubauer, F., Liu, X., Genser, J. & Hauzenberger, C. 2011b. Tectonic evolution of the Qinling orogen, China: review and synthesis. *Journal of Asian Earth Sciences* **41**(3), 213–37.

Enkelmann, E., Ratschbacher, L., Jonckheere, R., Nestler, R., Fleischer, M., Gloaguen, R., Hacker, B. R., Zhang, Y. Q. & Ma, Y. S. 2006. Cenozoic exhumation and deformation of northeastern Tibet and the Qinling: is Tibetan lower crustal flow diverging around the Sichuan Basin? *Geological Society of America Bulletin* **118**(5–6), 651–71.

Faure, M., Lin, W., Monié, P., Breton, N. L., Poussineau, S., Panis, D. & Deloule, E. 2003. Exhumation tectonics of the ultrahigh-pressure metamorphic rocks in the Qinling orogen in east China: new petrological-structural-radiometric insights from the Shandong Peninsula. *Tectonics* **22**(3), 127–43.

Glorie, S., Grave, J. D., Buslov, M. M., Elburg, M. A., Stockli, D. F., Gerdes, A. & Haute, P. V. D. 2010. Multi-method chronometric constraints on the evolution of the Northern Kyrgyz Tien Shan granitoids (Central Asian Orogenic Belt): from emplacement to exhumation. *Journal of Asian Earth Sciences* **38**(3–4), 131–46.

Grave, J. D., Buslov, M. M. & Haute, P. V. D. 2007. Distant effects of India–Eurasia convergence and Mesozoic intracontinental deformation in Central Asia: constraints from apatite fission-track thermochronology. *Journal of Asian Earth Sciences* **29**(2–3), 188–204.

Grave, J. D., Glorie, S., Buslov, M. M., Stockli, D. F., Mcwilliams, M. O., Batalev, V. Y. & Haute, P. V. D. 2013. Thermo-tectonic history of the Issyk-Kul basement (Kyrgyz Northern Tien Shan, Central Asia). *Gondwana Research* **23**(3), 998–1020.

Guo, Z. T., Ruddiman, W. F., Hao, Q. Z., Wu, H. B., Qiao, Y. S., Zhu, R. X., Peng, S. Z., Wei, J. J., Yuan, B. Y. & Liu, T. S. 2002. Onset of Asian desertification by 22 Myr ago inferred from loess deposits in China. *Nature* **416**(6877), 159–63.

Guo, Z. T., Sun, B., Zhang, Z. S., Peng, S. Z., Xiao, G. Q., Ge, J. Y., Hao, Q. Z., Qiao, Y. S., Liang, M. Y. & Liu, J. F. 2008. A major reorganization of Asian climate by the early Miocene. *Climate of the Past* **4**(3), 153–74.

Hacker, B. R., Ratschbacher, L., Webb, L., Ireland, T., Walker, D. & Dong, S. 1998. U/Pb zircon ages constrain the architecture of the ultrahigh-pressure Qinling–Dabie Orogen, China. *Earth & Planetary Science Letters* **161**(1), 215–30.

Hacker, B. R., Ratschbacher, L., Webb, L., McWilliams, M. O., Ireland, T., Calvert, A., Dong, S., Wenk, H. R. & Chateigner, D. 2000. Exhumation of ultrahigh-pressure continental crust in east central China: Late Triassic-Early Jurassic tectonic unroofing. *Journal of Geophysical Research Solid Earth* **105**, 13,339–64.

Heberer, B., Anzenbacher, T., Neubauer, F., Genser, J., Dong, Y. & Dunkl, I. 2014. Polyphase exhumation in the western Qinling Mountains, China: rapid Early Cretaceous cooling along a lithospheric-scale tear fault and pulsed Cenozoic uplift. *Tectonophysics* **617**(4), 31–43.

Hu, J. 2004. Mid-Late Palaeozoic extension of the Wudang block in the South Qinling tectonic belt, China. *Chinese Journal of Geology* **39**(3), 305–19.

Hu, S., Kohn, B. P., Raza, A., Wang, J. & Gleadow, A. J. W. 2006a. Cretaceous and Cenozoic cooling history across the ultrahigh pressure Tongbai–Dabie belt, central China, from apatite fission-track thermochronology. *Tectonophysics* **420**(3–4), 409–29.

Hu, S., Raza, A., Min, K., Kohn, B. P., Reiners, P. W., Ketcham, R. A., Wang, J. & Gleadow, A. J. W. 2006b. Late Mesozoic and Cenozoic thermotectonic evolution along a transect from the north China craton through the Qinling orogen into the Yangtze craton, central China. *Tectonics* **25**(6), 97–112.

Huang, W. 1993. Multiphase deformation and displacement within a basement complex on a continental margin: the Wudang Complex in the Qinling Orogen, China. *Tectonophysics* **224**(224), 305–26.

Huang, F., Li, S., Dong, F., Li, Q., Chen, F., Wang, Y. & Yang, W. 2007. Recycling of deeply subducted continental crust in the Dabie Mountains, central China. *Lithos* **96**(1–2), 151–69.

Hurford, A. J. & Green, P. F. 1983. The zeta age calibration of fission-track dating. *Chemical Geology* **41**(83), 285–317.

Jonckheere, R., Enkelmann, E., Min, M., Trautmann, C. & Ratschbacher, L. 2007. Confined fission tracks in ion-irradiated and step-etched prismatic sections of Durango apatite. *Chemical Geology* **242**(1), 202–17.

Jonckheere, R., Ratschbacher, L. & Wagner, G. A. 2003. A repositioning technique for counting induced fission tracks in muscovite external detectors in single-grain dating of minerals with low and inhomogeneous uranium concentrations. *Radiation Measurements* **37**(3), 217–9.

Ketcham, R. A. 2005. Forward and inverse modeling of low-temperature thermochronometry data. *Reviews in Mineralogy & Geochemistry* **58**(1), 275–314.

Ketcham, R. A., Balestrieri, M. L., Zattin, M. & Donelick, R. A. 2009. Reproducibility of apatite fission-track length data and thermal history reconstruction. *Earth & Planetary Science Letters* **284**(3), 504–15.

Ketcham, R. A., Donelick, R. A. & Carlson, W. D. 1999. Variability of apatite fission-tack annealing kinetics III: extrapolation to geological time scales. *American Mineralogist* **84**, 1235–55.

Kirby, E., Reiners, P. W., Krol, M. A., Whipple, K. X., Hodges, K. V., Farley, K. A., Tang, W. & Chen, Z. 2002. Late Cenozoic evolution of the eastern margin of the Tibetan Plateau: inferences from $^{40}Ar/^{39}Ar$ and (U-Th)/He thermochronology. *Tectonics* **21**(1), 1–20.

Kröner, A., Zhang, G. W. & Sun, Y. 1993. Granulites in the Tongbai Area, Qinling Belt, China: geochemistry, petrology, single zircon geochronology, and implications for the tectonic evolution of eastern Asia. *Tectonics* **12**(1), 245–55.

Li, S., Xiao, Y., Liou, D., Chen, Y., Ge, N., Zhang, Z., Sun, S. S., Cong, B., Zhang, R. & Hart, S. R. 1993. Collision of the North China and Yangtse Blocks and formation of coesite-bearing eclogites: timing and processes . *Chemical Geology* **109**(1–4), 89–111.

Li, X. H., Li, W. X., Wang, X. C., Li, Q. L., Liu, Y., Tang, G. Q., Gao, Y. Y. & Wu, F. Y. 2010. SIMS U–Pb

zircon geochronology of porphyry Cu–Au–(Mo) deposits in the Yangtze River Metallogenic Belt, eastern China: magmatic response to early Cretaceous lithospheric extension. *Lithos* **119**(3–4), 427–38.

Li, Z. X. & Li, X. H. 2007. Formation of the 1300-km-wide intracontinental orogen and postorogenic magmatic province in Mesozoic South China: a flat-slab subduction model. *Geology* **35**(2), 179–82.

Lin, X., Chen, H., Wyrwoll, K. H. & Cheng, X. 2010. Commencing uplift of the Liupan Shan since 9.5 Ma: evidences from the Sikouzi section at its east side. *Journal of Asian Earth Sciences* **37**(4), 350–60.

Ling, W. L., Duan, R. C., Liu, X. M., Cheng, J. P., Mao, X. W., Peng, L. H. & Liu, Z. X. 2008. Timing of the Wudangshan, Yaolinghe volcanic sequences and mafic sills in South Qinling: U-Pb zircon geochronology and tectonic implication. *Chinese Science Bulletin* **53**(14), 2192–9.

Ling, W. L., Duan, R. C., Liu, X. M., Cheng, J. P., Mao, X. W., Peng, L. H., Liu, Z. X., Yang, H. M. & Ren, B. F. 2010. U-Pb dating of detrital zircons from the Wudangshan Group in the South Qinling and its geological significance. *Chinese Science Bulletin* **55**(22), 2440–8.

Liu, J., Zhang, P., Lease, R. O., Zheng, D., Wan, J., Wang, W. & Zhang, H. 2012. Eocene onset and late Miocene acceleration of Cenozoic intracontinental extension in the North Qinling range–Weihe graben: insights from apatite fission track thermochronology. *Tectonophysics* **584**(1), 281–96.

Liu, M., Cui, X. & Liu, F. 2004. Cenozoic rifting and volcanism in eastern China: a mantle dynamic link to the Indo–Asian collision? *Tectonophysics* **393**(1), 29–42.

Macaulay, E. A., Sobel, E. R., Mikolaichuk, A., Kohn, B. & Stuart, F. M. 2014. Cenozoic deformation and exhumation history of the Central Kyrgyz Tien Shan. *Tectonics* **33**(2), 135–65.

Mattauer, M., Matte, P., Malavieille, J., Tapponnier, P., Maluski, H., Qin, X. Z., Lun, L. Y. & Qin, T. Y. 1985. Tectonics of the Qinling Belt: build-up and evolution of eastern Asia. *Nature* **317**(6037), 496–500.

McDougall, I. & Harrison, T. M. 1999. *Geochronology and thermochronology by the 40Ar/39Ar method*. Oxford: Oxford University Press, 269 pp.

McDowell, F. W., McIntosh, W. C. & Farley, K. A. 2005. A precise ^{40}Ar–^{39}Ar reference age for the Durango apatite (U–Th)/He and fission-track dating standard. *Chemical Geology* **214**(3), 249–63.

Molnar, P., Boos, W. R. & Battisti, D. S. 2010. Orographic controls on climate and paleoclimate of Asia: thermal and mechanical roles for the Tibetan Plateau. *Annual Review of Earth & Planetary Sciences* **38**(1), 77–102.

Okay, A. I., Şengör, A. M. C. & Satir, M. 1993. Tectonics of an ultrahigh-pressure metamorphic terrane: the Dabie Shan/Tongbai Shan Orogen, China. *Tectonics* **12**(6), 1320–34.

Ouimet, W., Whipple, K., Royden, L., Reiners, P., Hodges, K. & Pringle, M. 2010. Regional incision of the eastern margin of the Tibetan Plateau. *Lithosphere* **2**(1), 50–63.

Ratschbacher, L., Franz, L., Enkelmann, E., Jonckheere, R., Pörschke, A., Hacker, B. R., Dong, S. & Zhang, Y. 2006. The Sino-Korean–Yangtze suture, the Huwan detachment, and the Paleozoic–Tertiary exhumation of (ultra)high-pressure rocks along the Tongbai-Xinxian-Dabie Mountains. *Special Paper of the Geological Society of America* **403**, 45–75.

Ratschbacher, L., Hacker, B. R., Calvert, A., Webb, L. E., Grimmer, J. C., McWilliams, M. O., Ireland, T., Dong, S., Hu, J. & Calvert, A. 2003. Tectonics of the Qinling (Central China): tectonostratigraphy, geochronology, and deformation history. *Tectonophysics* **366**(1–2), 1–53.

Ratschbacher, L., Hacker, B. R., Webb, L. E., McWilliams, M., Ireland, T., Dong, S., Calvert, A., Chateigner, D. & Wenk, H. R. 2000. Exhumation of the ultrahigh-pressure continental crust in east central China: Cretaceous and Cenozoic unroofing and the Tan-Lu fault. *Journal of Geophysical Research Solid Earth* **105**(B6), 13,303–38.

Reiners, P. W., Spell, T. L., Nicolescu, S. & Zanetti, K. A. 2004. Zircon (U-Th)/He thermochronometry: He diffusion and comparisons with ^{40}Ar/^{39}Ar dating. *Geochimica et Cosmochimica Acta* **68**(8), 1857–87.

Richardson, N. J., Densmore, A. L., Seward, D., Fowler, A., Wipf, M., Ellis, M. A., Yong, L. & Zhang, Y. 2008. Extraordinary denudation in the Sichuan Basin: insights from low-temperature thermochronology adjacent to the eastern margin of the Tibetan Plateau. *Journal of Geophysical Research* **113**, B04409.doi: 10.1029/2006/JB004739.

Rowley, D. B., Xue, F., Tucker, R. D., Peng, Z. X., Baker, J. & Davis, A. 1997. Ages of ultrahigh pressure metamorphism and protolith orthogneisses from the eastern Dabie Shan: U/Pb zircon geochronology. *Earth & Planetary Science Letters* **151**(3–4), 191–203.

Şengör, A. M. C. 1985. Geology: East Asian tectonic collage. *Nature* **318**(6041), 16–7.

Sharp, W. D. & Clague, D. A. 2006. 50-Ma initiation of Hawaiian-Emperor bend records major change in Pacific plate motion. *Science* **313**(5791), 1281–4.

Shen, C., Mei, L., Min, K., Jonckheere, R., Ratschbacher, L., Yang, Z., Peng, L. & Liu, Z. 2012. Multi-chronometric dating of the Huarong granitoids from the middle Yangtze Craton: implications for the tectonic evolution of eastern China. *Journal of Asian Earth Sciences* **52**(3), 73–87.

Shen, C., Mei, L., Peng, L., Chen, Y., Yang, Z. & Hong, G. 2011. LA-ICPMS U–Pb zircon age constraints on the provenance of Cretaceous sediments in the Yichang area of the Jianghan Basin, central China. *Cretaceous Research* **34**(3), 172–83.

Shen, C. B., Mei, L. F. & Xu, S. H. 2009. Fission track dating of Mesozoic sandstones and its tectonic significance in the Eastern Sichuan Basin, China. *Radiation Measurements* **44**(9), 945–9.

Tada, R., Zheng, H. & Clift, P. D. 2016. Evolution and variability of the Asian monsoon and its potential linkage with uplift of the Himalaya and Tibetan Plateau. *Progress in Earth & Planetary Science* **3**(1), 1–26.

Tapponnier, P., Zhiqin, Xu, Roger, F., Meyer, B., Arnaud, N., Wittlinger, G. & Jingsui, Y. 2001. Oblique stepwise rise and growth of the Tibet plateau. *Science* **294**(5547), 1671–7.

Tian, Y., Kohn, B. P., Gleadow, A. J. W. & Hu, S. 2013. Constructing the Longmen Shan eastern Tibetan Plateau margin: insights from low-temperature thermochronology. *Tectonics* **32**(3), 576–92.

Tian, Y., Kohn, B. P., Hu, S. & Gleadow, A. J. W. 2015. Synchronous fluvial response to surface uplift in the eastern Tibetan Plateau: implications for crustal dynamics. *Geophysical Research Letters* **42**(1), 29–35.

Tian, Y., Kohn, B. P., Zhu, C., Xu, M., Hu, S. & Gleadow, A. J. W. 2012. Post-orogenic evolution of the Mesozoic

Micang Shan Foreland Basin system, central China. *Basin Research* **24**(1), 70–90.

Wang, X., Zattin, M., Li, J., Song, C., Peng, T., Liu, S. & Liu, B. 2011. Eocene to Pliocene exhumation history of the Tianshui-Huicheng region determined by apatite fission track thermochronology: implications for evolution of the northeastern Tibetan Plateau margin. *Journal of Asian Earth Sciences* **42**(1–2), 97–110.

Wu, F. Y., Lin, J. Q., Wilde, S. A., Zhang, X. O. & Yang, J. H. 2005. Nature and significance of the Early Cretaceous giant igneous event in eastern China. *Earth & Planetary Science Letters* **233**(1), 103–19.

Wu, T., Xiao, L. & Ma, C. 2016. U-Pb Geochronology of detrital and inherited zircons in the Yidun Arc Belt, Eastern Tibet Plateau and its tectonic implications. *Journal of Earth Science* **27**(3), 461–73.

Xia, L. Q., Xia, Z. C., Xiang-Min, L. I., Zhong-Ping, M. A. & Xue-Yi, X. U. 2008. Petrogenesis of the Yaolinghe Group,Yunxi Group,Wudangshan Group volcanic rocks and basic dyke swarms from eastern part of the South Qinling Mountains. *Northwestern Geology* **41**(3), 1–29.

Xie, G., Mao, J. & Zhao, H. 2011. Zircon U–Pb geochronological and Hf isotopic constraints on petrogenesis of Late Mesozoic intrusions in the southeast Hubei Province, Middle–Lower Yangtze River belt (MLYRB), East China. *Lithos* **125**(1–2), 693–710.

Xiong, F., Ma, C., Jiang, H. & Zhang, H. 2016. Geochronology and petrogenesis of Triassic high-K Calc-Alkaline granodiorites in the East Kunlun Orogen, West China: juvenile lower crustal melting during post-collisional extension. *Journal of Earth Science* **27**(3), 474–90.

Yang, Z. 2014. Geochronologic constraints on tectonics of the Qin and Daba Mountains. PhD Thesis. Technische Universität Bergakademie Freiberg, Freiberg, Germany. Published thesis.

Yang, Z., Ratschbacher, L., Jonckheere, R., Enkelmann, E., Dong, Y., Shen, C., Wiesinger, M. & Zhang, Q. 2013. Late-stage foreland growth of China's largest orogens (Qinling, Tibet): evidence from the Hannan-Micang crystalline massifs and the northern Sichuan Basin, central China. *Lithosphere* **5**(4), 420–37.

Yuan, D. Y., Ge, W. P., Chen, Z. W., Li, C. Y., Wang, Z. C., Zhang, H. P., Zhang, P. Z., Zheng, D. W., Zheng, W. J. & Craddock, W. H. 2013. The growth of northeastern Tibet and its relevance to large-scale continental geodynamics: a review of recent studies. *Tectonics* **32**(5), 1358–70.

Yue, S. W., Deng, X. H. & Bagas, L. 2014. Geology, isotope geochemistry, and ore genesis of the Yindonggou Ag–Au(–Pb–Zn) deposit, Hubei Province, China. *Geological Journal* **49**(4–5), 442–62.

Zhang, C., Ma, C. Q. & Holtz, F. 2010. Origin of high-Mg adakitic magmatic enclaves from the Meichuan pluton, southern Dabie orogen (cental China): implications for delamination of the lower continental crust and melt–mantle interaction. *Lithos* **119**(3–4), 467–84.

Zhang, C., Ma, C. Q., Liao, Q. A., Zhang, J. Y. & She, Z. B. 2011. Implications of subduction and subduction zone migration of the Paleo-Pacific Plate beneath eastern North China, based on distribution, geochronology, and geochemistry of Late Mesozoic volcanic rocks. *International Journal of Earth Sciences* **100**(7), 1665–84.

Zhang, P., Miao, Y., Zhang, Z., Lu, S., Zhang, Y., Chen, H., Li, X., Miao, Q., Feng, W. & Ou, J. 2013. Late Cenozoic sporopollen records in the Yangtze River Delta, East China and implications for East Asian summer monsoon evolution. *Palaeogeography Palaeoclimatology Palaeoecology* **388**(6), 153–65.

Zhang, Y. Q., Vergely, P. & Mercier, J. 1995. Active faulting in and along the Qinling Range (China) inferred from SPOT imagery analysis and extrusion tectonics of south China. *Tectonophysics* **243**(1), 69–95.

Zhang, Y., Zhang, J. & Huaikun, L. I. 2013. Zircon U-Pb geochronology of the meta-acidic volcanic rocks from the Wudangshan Group, Southern Qinling Mountains, Central China. *Acta Geologica Sinica* **61**(9), 4447–55.

Zhang, Z. Q., Zhang, G. W., Tang, S. H. & Wang, J. H. 2002. The age of metamorphic rocks of the Wudang Group. *Geology in China* **29**(2), 117–25.

Zhang, Z. B., Shen, C. B., Shao, C. & Liu, Z. Q. 2013. Tectonothermal evolution of the eastern Tibetan Plateau Foreland: fission-track thermochronology of the southern Dabashan Fold-Thrust Belt. *Journal of Earth Science* **24**(4), 479–90.

Zhao, H. X., Jiang, S. Y., Dai, B. Z., Ma, L. & Li, J. W. 2015. Geochronology and Hf isotope study of pegmatite in the Xiaoqinling Area of NW China: implication for petrogenesis and regional metamorphism. *Journal of Earth Science* **26**(3), 295–305.

Zhou, B. X., Sun, T., Shen, W., Shu, L. & Niu, Y. 2006. Petrogenesis of Mesozoic granitoids and volcanic rocks in South China: a response to tectonic evolution. *Episodes* **29**(1), 26.

Zhou, X. M. & Li, W. X. 2000. Origin of late Mesozoic igneous rocks in Southeastern China: implications for lithosphere subduction and underplating of mafic magmas. *Tectonophysics* **326**(3–4), 269–328.